Published in final edited form as:
J Am Chem Soc. 2010 December 8; 132(48): . doi:10.1021/ja107333g.

Polymer-Caged Nanobins for Synergistic Cisplatin-Doxorubicin Combination Chemotherapy

Sang-Min Lee, **Thomas V. O'Halloran**, and **SonBinh T. Nguyen**
Department of Chemistry and the Center of Cancer Nanotechnology Excellence, Northwestern University, 2145 Sheridan Road, Evanston, Illinois 60208-3113

Thomas V. O'Halloran: t-ohalloran@northwestern.edu; SonBinh T. Nguyen: stn@northwestern.edu

Abstract

Multicomponent chemotherapy has increasingly become a strategy of great importance in clinical cancer treatments. However, this type of chemotherapy has not been demonstrated in nanoscale delivery vehicles where two cytotoxic agents can be packaged together, potentially leading to synergistic drug activities. Herein, we present the co-delivery of doxorubicin and cisplatin via a single polymer-caged nanobin (PCN) and show that co-packaging can yield strong synergy in the efficacy of these agents. Such a PCN comprises of a doxorubicin-encapsulated liposomal core protected by a pH-responsive cisplatin prodrug-loaded polymer shell with tunable drug ratios and surface charge potentials. This dual-agent Pt-PCN$_{DXR}$ formulation dramatically enhances the overall cytotoxicity of each drug against cancer cells at reduced doses and exhibits higher synergy than combinations of either the free drugs or separately nano-packaged drugs. These results clearly indicate that the polymer-caged nanobin platform can offer new means for building synergy into combination chemotherapy regimens.

Keywords

nanoparticles; cancer; combination chemotherapy; cisplatin; doxorubicin

Introduction

In chemotherapy based on small-molecule drugs, the use of a single agent often fails to achieve complete cancer remission due to the rapid development of drug resistance in tumor cells.[1] Hence, most clinical regimens are comprised of multiple non-cross-resistant anticancer agents.[2] Among all available chemotherapeutic agents, the most commonly used are arguably anthracycline[3] and platinum-based drugs.[4,5] In the few cases where these two classes of drugs have been combined, enhanced tumor responses were observed in patients with ovarian cancer,[6] advanced breast cancer,[7] and endometrial carcinoma,[8] thus emphasizing the potential of this drug combination in the treatment of cancer.

Correspondence to: Thomas V. O'Halloran, t-ohalloran@northwestern.edu; SonBinh T. Nguyen, stn@northwestern.edu.

Supporting Information **Available**: Plots of hydrodynamic diameters of BL$_{DXR}$, PCN$_{DXR}$, and Pt-PCN$_{DXR}$; *in vitro* cytotoxicity profile of poly(acrylate); UV-vis analyses of *cis*-PtLys under acidic condition; MS analysis of the dialytes of Pt-PCNs; Proposed mechanism for Pt-release from the N_{α}-acetylamido ligand; comparison of cumulative release of Pt and DXR from Pt-PCN$_{DXR}$; complete list of combination index (C.I.) values for Pt-PCN$_{DXR}$ and free drug combination against OCVAR-3 and MDA-MB-231; dose-effect cytotoxicity profiles of Pt-PCN$_{DXR}$ against MCF-7 cells, the corresponding C.I-analyses, and apoptosis evaluations. This material is available free of charge via the Internet at http://pubs.acs.org.

DNA-modifying agents such as cisplatin (CDDP) and anthracycline-based topoisomerase II (TOP2)-inhibitors[9] have been explored in combination chemotherapy against human lung cancer cell lines and in the corresponding *in vivo* murine models where they show greatly enhanced activity.[10] These studies represent examples of drug synergism where the co-administration of two drugs leads to significantly greater activity than predicted from the simple addition of the effects of each drug component.[11-13] Such synergism arises because the inhibition of TOP2 can partially hinder the efficient repair of DNA damaged by alkylating agents[14] and has been observed to increase the efficacy of CDDP in human lung tumor xenografts,[10] human glioblastoma,[15] and leukemia cell line.[16] Indeed, co-administration of CDDP with TOP2-inhibitors such as doxorubicin (DXR) has improved the therapeutic efficacy in a phase III clinical trial in endometrial carcinoma;[8] however, this dosing regimen is limited by unfavorable side effects.

The side effects that accompany [DXR + CDDP] combination chemotherapy can potentially be reduced by encapsulating these small-molecule agents in nanoscale delivery platforms.[17,18] This approach has been shown to improve the therapeutic efficacy of toxic drugs by facilitating their selective accumulation at tumor sites over normal tissue, via enhanced permeation and retention effect, and protecting the drug payload against premature degradation and systemic clearance. For instance, PEGylated liposomal DXR (Doxil™) is a clinically successful nanoscale formulation that has been used to treat Kaposi's sarcoma and refractory breast and ovarian cancers.[19] While Doxil™ possesses a prolonged plasma half-life and absence of cardiotoxicity compared to the parent DXR drug, severe side effects remain when it is co-administrated with platinum drugs.[20-22] As such, if the co-delivery of DXR and CDDP can be engineered into a single nanoscale platform, the dose requirement could be lowered to reduce dose-limiting toxicity and increase antitumor activity.

Herein, we report a strong synergy in the efficacy of the [DXR + CDDP] drug combination when co-delivered to cancer cells via a single nanoparticle using our lipid-templated polymer-caged nanobin (PCN) platform. PCN can encapsulate a high density of therapeutic agent such as DXR inside the liposomal core[23] surrounded by a pH-responsive polymer cage[24] possessing modified Pt-prodrug at various Pt/DXR ratios (Scheme 1). Through this Pt-conjugated, DXR-encapsulated PCN (Pt-PCN_{DXR}), both drugs can be co-delivered via a single particle, potentially giving rise to enhanced therapeutic efficacy in comparison to the free drug combinations. Indeed, we observed highly synergistic potency of the two drugs in the Pt-PCN_{DXR} formulation against several cancer cell lines at significantly lower doses than those observed when DXR and CDDP are combined in free-drug forms or separately packaged nanoparticles.

Results and Discussion

Synthesis and release profiles of Pt-PCN_{DXR}

We have previously reported the synthesis of DXR-loaded PCN (PCN_{DXR}) using a two-step protocols: 1) insertion of monodisperse cholesterol-terminated poly(acrylic acid) chains into the lipid bilayer of a doxorubicin-loaded bare liposome and 2) *in situ* cross-linking with diamine linkers to form PCN_{DXR} (Scheme 1).[23] The resulting PCN_{DXR} can effectively release DXR at the low pH commonly found in solid tumor environments[25] and exhibit excellent cytotoxicity against several types of cancer cells. Relevant to the present study, the polymer cage of the PCN_{DXR} still has a significant number of free carboxylic acid groups (see estimate below), allowing for the subsequent conjugation of Pt-prodrug onto its shell.

In the present study, cholesterol-terminated poly(acrylic acid) (M_n ~5,100 Da; as controls, poly(acrylic acid) chains with molecular weight of 2-5 kDa exhibited no apparent *in vitro* toxicity up to 300 μM, see Figure S2 in SI) was employed in the synthesis of PCN_{DXR}. A

cisplatin prodrug, *cis*-[$Pt^{II}(NH_3)_2(N_\alpha$-AcLys)] (*cis*-PtLys, Scheme 2), is then tethered onto the unreacted carboxyl groups on the polymer cage through the C6-amine moiety of lysine, affording Pt-PCN_{DXR} with tunable Pt/lipid molar ratio ranging from 0.02 to 1.29 (Pt/DXR = 0.1-5.9, ~129,000 Pt atoms per particle; at ~10,000 polymer chains per liposome and 50% cross-links, up to 300,000 free carboxylic acid groups are theoretically available for conjugation of the prodrug). Consistent with the modification of the PCN polymer shell with small molecules, the hydrodynamic diameters of the resulting Pt-PCN_{DXR} (128 ± 16 nm) are essentially unchanged from that of the parent PCN_{DXR} (125 ± 14 nm, Figure S1 in Supporting Information (SI)). As expected, the zeta (ζ) potential of Pt-PCN_{DXR} dramatically changes as the level of modification increases, from -14.4 mV for the parent PCN_{DXR} at neutral condition, where most the carboxyl groups on the shells are negatively charged, to 1.4 mV for the amide-conjugated Pt-PCN_{DXR} with Pt/lipid ratio of 1.29 (Figure 1A). In comparison, mixtures of *cis*-PtLys and PCN_{DXR} without amide-conjugation still exhibit overall negative zeta potential over a wide range of Pt/lipid ratio. Such conversion of free carboxylate groups into covalent amide linkages in Pt-PCN_{DXR} lead to nanoparticles with near-neutral surface charge that are expected to undergo less opsonization than charged species during *in vivo* circulation,[26] and thus will have longer plasma circulation time.

Drug delivery vehicles are often ineffective if their payload cannot be triggered-released at the disease site, thus decreasing the overall therapeutic efficacy of the packaged drugs. Indeed, CDDP-loaded PEGylated liposome with negligible drug-releasing profiles[27] was found to have low therapeutic efficacy both in tumor models *in vivo*[27,28] and in clinical trials.[29,30] To this end, we evaluated the release rates of platinum from Pt-PCN via dialysis against saline buffer solutions at physiological (pH 7.4) and acidic (pH 5.0) pHs at 37 °C to mimic the acidic environment in tumor interstitium[25] and cellular endosomes.[31] As expected for the *cis*-PtLys prodrug, which shows characteristic UV-vis absorption change under acidic condition (Section S1 in SI), the Pt-release kinetics of Pt-PCNs was pH-tunable (Figure 1B): Pt-PCN was relatively inert at pH 7.4, with only ~15% of Pt released after 72 h; while at pH 5.0, ~50% Pt was released during the initial 36 h and ~65% release was achieved after 72 h. This observed acid-sensitive release of Pt^{II} ions from the PCN shell can be attributed to the acid lability of the N_α-acetylamido ligand,[32,33] which is protonated by acid and dechelate from the Pt center, eventually leading to an easy release of Pt^{II} ions as a diamminediaquo Pt complex (Figure S4 and Section S1 in SI). In conjunction with the previously reported acid-sensitive DXR-release from PCN_{DXR} (Figure S5 in SI),[23] the enhanced release of platinum from Pt-PCN at low pH can be advantageous in the *in vivo* treatment of solid tumor tissues whose environments are often acidic.[25]

Cytotoxicity and synergism profiles of Pt-PCN_{DXR}

The anti-tumor effect of the [*cis*-PtLys + DXR] combination in Pt-PCN_{DXR} possessing various Pt/DXR ratios (Table 1) was initially evaluated using the OVCAR-3 ovarian cancer cell line. Pt-PCN_{DXR} exhibits a robust enhancement of combination potency, with dose-effect profiles shifted toward lower drug concentration as the Pt/DXR ratio increased (Figure 2A). Pt-PCN_{DXR} with high Pt/DXR molar ratio (5.9) showed better potency ($IC_{50}^{DXR}=0.90\mu M$ with $IC_{50}^{Pt}=7.1\mu M$) than free DXR ($IC_{50}^{DXR}=1.24\mu M$). Given that the IC_{50}^{Pt} of Pt-conjugated empty PCN without DXR (Pt-PCN_{emp}) alone was 66.1 μM (Figure 3A and Table 2), nine times higher than the IC_{50}^{Pt} (7.1 μM) for the Pt-PCN_{DXR} formulation, these data suggest synergistic cytotoxicity for both agents in Pt-PCN_{DXR} against OVCAR-3 cells.

To confirm drug synergy in Pt-PCN_{DXR}, we carried out combination index (C.I.) determinations and isobologram analyses.[11-13] In C.I. plots, combination index, derived from the dose-effect profiles of a given drug combination, were plotted against drug effect

levels. Such a plot can provide quantitative information about the extent of drug interactions, with C.I. values lower than, equal to, or higher than 1 denoting synergism, additivity, or antagonism, respectively. As shown in Figure 2C, C.I. plots for Pt-PCN_{DXR} clearly demonstrated higher synergism against OVCAR-3 cells over a wide range of drug effect levels (IC_{75} through IC_{25}) compared to the free drug combinations, which led to only mild synergism at comparable Pt/DXR ratios (Tables 1). Supporting this conclusion is the isobologram analysis for OVCAR-3 cells at IC_{50}, which shows very different profiles for Pt-PCN_{DXR} in comparison to the [CDDP + DXR] combination (Figure 2E). Because isobologram analysis shows only the combination ratio of each drug capable of producing a specified effect (50% cell death for IC_{50}),[11-13] it represents the combined drug effects more accurately than the logarithmic C.I. plots: as the iso-effect level of Pt-PCN_{DXR} is lower than that of free drug combination, higher synergism was clearly apparent for Pt-PCN_{DXR} using this analysis, supporting the dose-effect analysis described above.

The enhanced potency of the [*cis*-PtLys + DXR] combination in Pt-PCN_{DXR} was most apparent against MDA-MB-231 human breast cancer cells (Figure 2B). MDA-MB-231 cells are partially resistant to CDDP (Figure 3B and Table 2),[34] and thus the activity of the [CDDP + DXR] free drug combinations ranged from additive to antagonistic, depending on the Pt/DXR ratio (Figure 2D). In sharp contrast, co-packaging in Pt-PCN_{DXR} rendered the [Pt + DXR] drug combination synergistic: a highly attenuated C.I. value (C.I. = 0.34) was observed with Pt-PCN_{DXR} compared to that of the [CDDP + DXR] free drug combination (C.I. = 2.08) at the same Pt/DXR ratio (5.1, see Table 1), showing highly enhanced synergism with Pt-PCN_{DXR}. Isobologram analysis also shows significant synergy of the two drug components in Pt-PCN_{DXR}, in contrast to the antagonistic free drug combinations (Figure 2F).

The benefits of drug co-encapsulation

The synergism between DXR and Pt-prodrug in Pt-PCN_{DXR} was best demonstrated when compared to separately packaged drugs. Treatment of MDA-MB-231 cells with [Pt-PCN_{emp} + PCN_{DXR}], a mixture of two types of PCNs each containing only one drug, at Pt/DXR = 5.1, the drug ratio that yielded the best efficacy in Pt-PCN_{DXR}, demonstrated synergism at low drug effect levels ($\sim IC_{75}$) but became increasingly antagonistic at high drug effect levels (IC_{25}) (Figures 4, A and B). In contrast, the combined agent, Pt-PCN_{DXR}, administered at the same Pt/DXR ratio, remained highly synergistic over a wide range of IC values. This intriguing result clearly suggests that combining both drugs into a single nanoparticle can lead to a pronounced synergy in anticancer activity that is not seen when the bioactive components of Pt-PCN_{DXR} are administered as a simple mixture, either as free drugs or packaged individually in separate nanobins.

We note in passing that synergism in combination therapy has only been reported on case-by-case basis,[2] partly because synergism in combination therapy depends on many parameters such as the therapeutic mechanism of the individual drugs and the phenotypes of target cell lines. In addition, the results of multi-component therapy can be strongly dependent on the dosing period and combination ratio of each drug even in one pair of drug combination. As such, although the excellent promises of synergistic combination therapy via co-delivery has been demonstrated here for the [DXR + CDDP] combination, more studies will be needed with other drug combinations to fully exploit the potential of the PCN platform.

Mechanisms of uptake and release

In dosing MDA-MB-231 cells with the [Pt-PCN_{emp} + PCN_{DXR}] combination, it is possible that the endocytotic uptake of each drug would be diluted by having about twice as many

nanobins as in the Pt-PCN_{DXR} case. Consistent with this hypothesis, the level of DXR uptake for the cells exposed to the [Pt-PCN_{emp} + PCN_{DXR}] combination is about half of the uptake level in cells treated with Pt-PCN_{DXR} at the same drug concentration (Figure 4C). Surprisingly, the amount of Pt uptake was similar in both treatments. This can be explained by the more negative zeta potential of PCN_{DXR} ($\zeta = -14.4$ mV), which results in less uptake compared to Pt-PCN_{emp} and Pt-PCN_{DXR} ($\zeta = 1.4$ mV for both).[35] Thus, when the two drugs are combined into one platform, the DXR core can now take advantage of the near-neutral surface charge of the Pt-loaded shell, leading to enhanced physical uptake and superior therapeutic efficacy. Coupled to the known preference of nano-packaged drugs to localize into the cell's organelles,[36] our results have significant clinical implications in the multi-agent chemotherapeutic treatment of cancer patients with resistant or refractory disease. The selective partition of nano-packaged drugs into the sub-cellular organelles can retain the drug molecules in the tumor longer by keeping them away from the cellular efflux pumps that are present in many types of drug-resistant cells.[17,18] Simultaneously, the synergistically enhanced efficacy of the co-delivered drugs would accelerate cell deaths, killing the tumor more effectively than the corresponding combination of free drugs.

Release of Pt-pharmacophore and apoptosis assay

The clinically used small-molecule version of platinum drugs typically induce apoptosis (i.e., programmed cell death) by cross-linking DNA in many cancer cells.[4] Therefore, we gauged the therapeutic activity of Pt-PCN_{emp} by their capability to induce apoptosis in cancer cells. The CDDP-sensitive OVCAR-3 human ovarian carcinoma cells were exposed to CDDP, Pt-PCN_{emp}, and *cis*-PtLys ([Pt] = 20 μM), for 48 h. Their Pt-induced apoptotic capabilities were then assessed using the Annexin-V/7-AAD assay, which is commonly used to monitor early apoptotic activity.[37] We were please to observe robust sensitization of cells by Pt-PCN_{emp}: ∼29% of cell populations were found to be at early apoptotic stages when exposed to Pt-PCN_{emp} compared to only ∼3-5% of early apoptosis for untreated or *cis*-PtLys-treated cells (Figures 5A and S6 in SI). This activity is comparable to that observed for CDDP-treated cells at the same [Pt] (∼25% apoptotic population). Upon treatment with Pt-PCN_{emp}, the apoptotic cell population also increases in a dose-dependent fashion[38] (Figure 5B), suggesting that the therapeutic potential of Pt-PCN_{emp} is primarily attributed to the pro-apoptotic activity of the active platinum moieties released from Pt-PCN_{emp}.

The observed different cytotoxicity of Pt-PCN_{emp} and free *cis*-PtLys can be attributed to different cellular uptake mechanisms. When OVCAR-3 cells were exposed to each drug formulation for 4 h at 20 μM [Pt] and then lysed to quantify the amount of intracellular Pt (Figure 5C), cells that were exposed to free *cis*-PtLys accumulated ∼0.027 fmol Pt/cell, only half the amount observed for those exposed to CDDP (∼0.05 fmol Pt/cell). Although the exact cellular uptake mechanism of CDDP is still being debated,[39] the lower accumulation of *cis*-PtLys can be attributed to its reduced lipophilicity, a consequence of its charged N_{α}-AcLys ligand at physiological condition. In contrast, the Pt accumulation in the cells that were exposed to Pt-PCN_{emp} (∼2.24 fmol Pt/cell) is 45 times higher than that in cells treated with CDDP and > 70 times higher than that in cells treated with *cis*-PtLys. Such stark contrast can be attributed to endocytosis, a well-known cellular uptake mechanism for nanoparticles.[36,40] After endocytotic uptake of Pt-PCN_{emp}, the acidic endosomal environments[31] can also enhance the release of active diaquo-Pt^{II} species from the Pt-PCN_{emp}, leading to the increased induction of apoptosis.

The apoptotic activities of the various formulations shown in Figure 5 can be understood in terms of both Pt uptake and diaquo-Pt^{II} release rate: The hydrolysis of Cl^- ions from CDDP allows the formation of aquo-Pt^{II} species inside the cells, leading to high potency with large population of dead cells (35.6%, Figure 5A) in our Annexin-V/7-AAD assay. In contrast,

negligible toxicity (8.1% cell death and 5.4% apoptosis) was observed for *cis*-PtLys, which may arise from the slow rate of amido ligand dissociation at the neutral pH of the cytosol (Figure 1B). However, because Pt-PCN$_{emp}$ were uptaken via endocytosis, the high acidity inside the endosome can mediate the controlled dechelation of the N_{α}-AcLys ligand better, leading to a higher release of the active Pt species in comparison to that of free *cis*-PtLys. Together with the high endocytotic Pt uptake of Pt-PCN$_{emp}$ (~45 times higher than that of CDDP), this higher release of the active diaquo-Pt^{II} species allows for Pt-PCN$_{emp}$ to have an apoptotic capability (29.4%) comparable to that of CDDP (24.7%). This enhanced cellular uptake-controlled release profile of Pt-PCNs may be highly advantageous in *in vivo* cancer therapy associated with the enhanced permeation and retention (EPR) effects in solid tumors.[41]

The enhanced cellular uptake and acid-triggered release of Pt^{II} via Pt-PCN$_{emp}$ is clearly responsible for the higher *in vitro* potency of Pt-PCN$_{emp}$ compared to free *cis*-PtLys. When screened against CDDP-sensitive OVCAR-3 and partially resistant MDA-MB-231 and MCF-7 human breast cancer cells,[34] no significant toxicity was observed in the cells treated with free *cis*-PtLys, up to 200 μM [Pt], as evaluated using the MTS cell proliferation assay (Figure 3A). However, the potency of Pt-PCN$_{emp}$ was significantly higher than the free *cis*-PtLys, with half-maximal inhibitory concentrations (IC_{50} = 66.1 μM for OVCAR-3, 106.6 μM for MCF-7, and 125.1 μM for MDA-MB-231) that are lower than the free drug. Because Pt-PCN$_{emp}$ exhibits relatively moderate toxicity compared to the high amounts of Pt uptake (i.e., cell-associated Pt), it is possible that some portion of Pt-drug can be still entrapped inside the endosomal vesicles or cytosol after the internalization. On the other hand, it is also possible that most of the Pt ions are still trapped in the polymer shell of the nanobins as *cis*-PtLys. Indeed, when we compared the apoptosis-inducing capability of Pt-PCN$_{emp}$ to that of CDDP using Annexin-V/7-AAD assay, Pt-PCN$_{emp}$ acts much more slowly due to the slow release property of Pt-pharmacophore (Figure 1B) even though comparable levels of apoptosis are induced by both drugs. The enhanced cytotoxicity of Pt-PCN$_{emp}$, together with its increased cellular accumulation, confirms that the Pt-prodrug can be effectively internalized into cells via nanoscale platforms, as has been observed for Pt-loaded lipid nanocapsules,[42] polymer nanoparticles,[43] and carbon nanotubes.[44]

Conclusion

In summary, we have shown that the therapeutic efficacy of cisplatin and DXR can be greatly enhanced in a synergistic fashion when co-delivered in the PCN platform, which combines the high DXR-loading capacity of liposomes with the synthetic tunability of a polymer shell that can serve as a reservoir for a Pt prodrug. The resulting Pt-PCN$_{DXR}$, having near-neutral surface charge, can be easily uptaken by cells via endocytosis, preserving the initial drug-combination ratio pre-determined for the excellent synergy during the cellular uptake process. Subsequently, triggered drug-releasing characteristics of PCN in acidic environment can lead to enhanced drug activity with superior synergism compared to either the free drug combinations or separately nano-packaged drugs. These results suggest that the PCN platform can provide a new way to achieve highly synergistic combinational chemotherapies. In addition, because drug-encapsulation in nano-platform can generally attenuate the acute toxicity of the parent drugs,[45] adverse systemic toxicity can also be substantially reduced. Such combined synergistic potency and reduced toxicity can be highly beneficial for cancer therapy and should be further enhanced by the conjugation of active targeting ligands.[46]

Experimental Section

Materials

1,2-dipalmitoyl-*sn*-glycero-3-phosphocholine (DPPC) and 1,2-dioleoyl-*sn*-glycero-3-[phospho-*rac*-(1-glycerol)] (sodium salt) (DOPG) were purchased from Avanti Polar Lipids (Alabaster, AL). Roswell Park Memorial Institute-1640 (RPMI-1640) medium and Eagle's Minimum Essential Medium (EMEM) were purchased from ATCC (Manassas, VA). Trypsin solution (0.25%, containing EDTA) was purchased from Invitrogen (San Diego, CA). Penicillin-streptomycin and phosphate-buffered saline (PBS) solutions were purchased from Mediatech (Manassas, VA). ICP calibration standard solutions for phosphorus and platinum, *N*-(3-Dimethylaminopropyl)-*N*′-ethylcarbodiimide hydrochloride, $Pt(NH_3)_2Cl_2$, N_α-acetyl-lysine, and all other reagents were purchased from the Aldrich Chemical Company (Milwaukee, WI) and used as received. Cholesterol-terminated poly(acrylic acid) was prepared using a literature procedure.[24] Ultrapure deionized (D.I.) water was obtained from a Millipore Biocel Milli-Q system (18.2 MΩ cm resistivity).

Measurements

Fourier-transformed nuclear magnetic resonance (NMR) spectroscopy was performed on a Varian INOVA-500 MHz spectrometer. Chemical shifts of ^1H NMR spectra are reported in ppm against residual solvent resonance as the internal standard ($CHCl_3$ = 7.27 ppm, CHD_2COCD_3 = 2.05 ppm, CHD_2OD = 3.31 ppm, D_2O = 4.8 ppm). UV-vis absorption spectra were obtained on a CARY 300 Bio UV-vis spectrophotometer.

Electrospray-ionization mass spectrometric (ESIMS) data were obtained on a Micromass Quattro II triple quadrupole mass spectrometer. Phosphorus and platinum concentrations of the synthesized materials and in bench-top release experiments were determined using a Varian Vista MPX simultaneous inductively coupled plasma optical emission spectrometer (ICP-OES). Numbers of platinum atoms internalized in the cells were measured by inductively coupled plasma mass spectroscopy (ICP-MS, X Series II, Thermo Electron) after digesting the cell pellets with concentrated nitric acid (100 μL, trace metal grade, Fisher Scientific) overnight.

Polymer molecular weights were measured relative to polystyrene standards on a Waters gelpermeation chromatograph (GPC) equipped with Breeze software, a 717 autosampler, Shodex KF-G guard column, KF-803L and KF-806L columns in series, a Waters 2440 UV detector, and a 410 RI detector. HPLC-grade THF was used as an eluent at a flow rate of 1.0 mL/min and the instrument was calibrated using polystyrene standards (Aldrich, 15 standards, 760-1,800,000 Daltons).

Dynamic light scattering (DLS) and zeta potential measurements were performed on a Zetasizer Nano ZS (Marvern Instruments, Malvern, UK) with a He-Ne laser (633 nm). Non-invasive backscatter method (detection at 173° scattering angle) was used. Correlation data were fitted, using the method of cumulants, to the logarithm of the correlation function, yielding the diffusion coefficient, *D*. The hydrodynamic diameters (D_H) of the BLs and PCNs were calculated using *D* and the Stokes-Einstein equation ($D_H = k_BT/3\pi\eta D$, where k_B is the Boltzmann constant, *T* is the absolute temperature, and η is the solvent viscosity (η = 0.8872 cP for water)). The polydispersity index (PDI) of liposomes— represented as $2c/b^2$, where *b* and *c* are first- and second-order coefficients, respectively, in a polynomial of a semi-log correlation function—was calculated by the cumulants analysis. Size distribution of vesicles was obtained by non-negative least squares (NNLS) analysis.[47] Unless noted otherwise, all samples were dispersed in 10-mM HEPES solution (pH 7.4, 150-mM NaCl)

for the measurements. The data reported represent an average of ten measurements with five scans each.

For *in vitro* assays, drug solutions were transferred with Beckman Coulter Biomek FX 96 multichannel robotic liquid handler (Beckman Coulter, Brea, CA) and MTS cell proliferation assays were monitored by Analyst GT Multimode Reader (Molecular Devices, Sunnyvale, CA) at NU High Throughput Analysis Laboratory (NU-HTA).

Preparation of *cis*-[Pt(NH$_3$)$_2$(N_α-acetyl-lysine)] (*cis*-PtLys)

cis-[Pt(NH$_3$)$_2$(N_α-acetyl-lysine)] was prepared using a modified literature procedure.[32] To a test tube (12 × 75 mm) equipped with a magnetic stirbar was added cisplatin (*cis*-Pt(NH$_3$)$_2$Cl$_2$, 60 mg, 200 μmol) dissolved in warm water. To the resulting solution was added silver nitrate (68 mg, 400 μmol, 2 equiv) with trace amount of nitric acid and the reaction mixture was allowed to stir for 3 days at room temperature in the dark. To completely precipitate out the slowly forming silver chloride, the solution was stored at 4 °C overnight. The completion of reaction can be determined by addition of small amount of NaCl solution to the aliquot of reaction mixture. After silver chloride precipitate was removed by filtration using centrifugal filter followed by syringe filter (pore size = 0.1 μm), N_α-acetyl-lysine (37.6 mg, 200 μmol) was added and allowed to stir for another 48 h at 50 °C in the dark. As the pH of reaction mixture decreased (pH < 3.0) due to the generation of proton from the N_α-acetyl-lysine ligand coordinated to Pt^{II} metal, the reaction progress can be monitored by checking pH during the reaction. To complete the reaction, pH should be adjusted below 5.0 by the addition of diluted NaOH solution. When pH increases above ∼5.0, hydroxide-bridged diplatinum complexes were formed as irreversible black precipitates.[48] Yellowish white solid was then collected and dried in air. The unoptimized yield was 17%. The desired *cis*-[Pt(NH$_3$)$_2$(N_α-AcLys)] complex was characterized by ^{1}H-NMR and ^{13}C-NMR spectroscopies (Figure 6A), and ESIMS (Figure 6B).

Preparation of Doxorubicin-loaded Polymer-Caged Nanobins (PCN$_{DXR}$)

Doxorubicin-loaded bare liposome was prepared using a modified literature procedure.[49] Briefly, to a cylindrical glass vial (15 mm × 45 mm) was added DPPC (18.048 μmol), DOPG (1.152 μmol), and cholesterol (12.8 μmol), followed by chloroform (0.5 mL) to make a colorless solution. After vortexing (30 sec), the solvent was removed by passing a stream of nitrogen over the solution while the vial was warmed in a 50 °C water bath. The resulting dry film was further dried under vacuum on a Schlenk line (< 30 mTorr) for one hour. Next, the dry lipid films were hydrated in 250 mM aqueous ammonium sulfate solution (500 μL) followed by vigorous vortexing (3-5 min on a Vortex Mixer, American Scientific Products) to form a dispersion of multilamellar vesicles. After this dispersion was subjected to 10 freeze-thaw cycles, it was extruded ten times through two stacked polycarbonate extrusion membranes (100-nm pore-size) that are maintained at 50 °C in a mini-extruder (Avanti Polar Lipids). The excess ammonium sulfate outside liposome was removed by Sephadex G-50 (10 mL) gel-filtration chromatography pre-equilibrated with 150-mM NaCl solution. To the collected liposome solution (∼ 600-800 μL of a solution with 4 mM lipid concentration) was added doxorubicin (DXR, 0.35 equiv of the total lipid content) followed by incubation at 50 °C for 24 h. The excess DXR outside of the liposome was then removed by passing the mixture through a column packed with Dowex 50WX4 cation-exchange resin (5 mL total resin volume, pre-cleaned with ultrapure deionized water).

The loading of the DXR was determined by breaking up the DXR-loaded liposome in a 75-mM HCl solution in 90% 2-propanol and measuring the dissolved doxorubicin concentration using UV-vis spectroscopy based on the extinction coefficient (ε) of DXR (11207 $M^{-1}cm^{-1}$ at λ_{max} = 480 nm). Mean hydrodynamic diameter (D_H) of 98 ± 12 nm was determined by

DLS measurements (Figure S1 in SI). The DXR-loaded bare liposomes (BL_{DXR}) was next subjected to the PCN fabrication process as reported previously.[24] For this process, 10 mol % of the Chol-PAA modifier was chosen to maximize the amount of the modifier while preventing local phase-segregation of all the cholesterol in the membrane. Additionally, 50% of acrylate repeating units in Chol-PAA chains were cross-linked with diamine cross-linker (25 mol%). Mean D_H of 125 ± 14 nm (Figure S1 in SI) and -14.4 mV of zeta potential (Figure 1A) was determined by DLS measurements. The resulting DXR-loaded PCN (PCN_{DXR}) can then be used directly in the conjugation with Pt-prodrug (see below).

Preparation of Pt-conjugated, doxorubicin-loaded polymer-caged nanobins (Pt-PCN_{DXR})

To a PCN_{DXR} solution ([lipid] = 10.5 mM) was added *N*-(3-dimethylaminopropyl)-*N*'-ethylcarbodiimide hydrochloride (8.3 mg, 14.4 μM) followed by the addition of *cis*-PtLys. As-prepared Pt-conjugated, DXR-loaded PCNs were purified by Sephadex G-50 (10 mL) gel-filtration chromatography pre-equilibrated with 20-mM HEPES buffer solution (pH 7.4, 150 mM NaCl). The loading efficiency of DXR and Pt was determined by using UV-vis spectroscopy and inductively coupled plasma optical emission spectroscopy (ICP-OES). Mean hydrodynamic diameter and zeta-potentials were determined by dynamic light scattering (DLS, Figure S1 in SI). The final Pt-to-lipid ratio is highly dependent on many parameters such as DP(X00304) (degree of polymerization) of polymer, polymer-insertion yield, and degree of cross-linking of the PCN preparation. Hence, each step in preparation can be precisely monitored by zeta potential measurements.[50]

Pt-release assay from Pt-PCNs

Pt-PCNs solutions (1 mM, 2 mL) were added into a semi-permeable dialysis tube (molecular weight cut-off 10 kDa) and dialyzed against either 20-mM acetate buffer (pH 5.0, 150 mM NaCl) or 20-mM HEPES buffer (pH 7.4, 150 mM NaCl) at 37 °C with stirring. An aliquot of the Pt-PCNs was collected at a pre-determined time and the phosphorus and platinum contents were measured by ICP-OES. The extent of Pt-release was observed by comparing time-dependent change of Pt/P molar ratio to the initial Pt/P value.

Cell culture

a. Medium—Roswell Park Memorial Institute (RPMI)-1640 cell culture medium (containing (L)-glutamine and phenol red) and trypsin solution (0.25%, containing EDTA) were purchased from Invitrogen (San Diego, CA). Eagle's Minimum Essential Medium (EMEM) was purchased from ATCC (Manassas, VA). Penicillin-streptomycin and phosphate-buffered saline (PBS, 1× without calcium and magnesium) solutions were purchased from Mediatech (Manassas, VA).

b. Cell lines—OVCAR-3 ovarian cancer cells were continuously cultured in RPMI-1640 medium supplemented with 10 vol% heat-inactivated fetal bovine serum (FBS, ATCC, Manassas, VA) and 0.5 vol% penicillin-streptomycin solution at 37 °C in a humidified atmosphere containing 5% CO_2. Human triple-negative MDA-MB-231 basal-like breast cancer cells were continuously cultured in EMEM supplemented with 10 vol% heat-inactivated fetal bovine serum (FBS) and 0.5 vol% penicillin-streptomycin solution at 37 °C in a humidified atmosphere containing 5% CO_2.

In vitro apoptosis assay

Flow cytometry with a Guava Nexin™ Apoptosis Assay kit (Annexin V-PE/7-AAD, Millipore) was used to determine apoptotic cell population. OVCAR-3 cells (100,000 cells) were seeded into a 24-well tissue culture plate and incubated for 24 h under standard growth conditions. Cell-growth media was then replaced with fresh media including Pt-PCNs (10,

20, 50, 100 μM), *cis*-PtLys (20 μM), or CDDP (20 μM). The drug-treated cells were incubated at 37 °C for 48 h in a humidified atmosphere containing 5% CO_2, after which the cells were washed with PBS buffer. The cells were then detached by harvesting with 0.25 % trypsin-EDTA solution and subsequently stained by the Guava Nexin reagent. Then the apoptotic cell population was measured using a Guava EasyCyte Mini flow cytometer. The data reported represent an average of three measurements from different batches.

In Vitro cellular Pt- and DXR-uptake measurements

OVCAR-3 cells (5×10^5 cells) were plated in two 6-well plates for 24 h before experiment (plate 1 for quantification of Pt and plate 2 for cell counting). Cells were exposed to Pt-PCNs, *cis*-PtLys, CDDP ([Pt] = 20 μM) for 4 h and washed with cold PBS buffer (3 × 2 mL). After trypsinized, each cell line was washed with cold PBS (2 mL/well) and pelleted using centrifugation (1500 rpm (500 g, Beckman-Coulter Allegra 6R Centrifuge), 4 °C, 5 min). After removing the supernatant, cells were resuspended in cold (4 °C) PBS solution (2 mL) followed by centrifugation. After washing by suspension/centrifugation process three times, cells from plate 1 were solubilized by adding an aqueous solution of Triton-X 100 (5 vol%, ∼10 μL or more until the cells are completely dissolved) and diluted to 200 μL total volume with ultrapure deionized water. Cell pellets from each well were digested with concentrated nitric acid (100 μL) before the Pt concentration is measured using inductively coupled plasma mass spectroscopy (ICP-MS). The numbers of Pt molecules per cell were determined against the total number of cells obtained with Guava ViaCount Assay using the samples from plate 2. The relative amount of DXR uptake was determined using fluorescent spectroscopy following our previously reported protocol.[23]

Cytotoxicity assays

The cells (20,000 cells) were seeded into 96-well plates (100 μL/well). The plates were then returned to the incubator (37 °C in a humidified atmosphere containing 5% CO_2) and the cells were allowed to grow to confluence for 24 h. The media in the wells were replaced with the pre-prepared growth media containing the appropriate drug formulation (100 μL of solution at the appropriate Pt and DXR concentrations). The drug-treated cells were incubated at 37 °C for either 48 h or 72 h in a humidified atmosphere containing 5% CO_2, after which the cells were washed with PBS buffer (2 × 150 μL).

The cell viabilities were then measured by MTS cell proliferation assay and the relative cell survival percentages compared to the drug-free control were plotted against the drug concentration in logarithmic scale. The data reported represent an average of three measurements from different batches. The dose-effect profiles were obtained by sigmoidal logistic fitting using *Origin 6.1* (OriginLab, Northampton, MA) and the half-maximal inhibitory concentration (IC_{50}) values were determined on the basis of the fitted data.

Supplementary Material

Refer to Web version on PubMed Central for supplementary material.

Acknowledgments

Financial support by the NIH (NCI Center of Cancer Nanotechnology Excellence U54CA119341 Project 4 and Core Grant P30CA060553 to the Robert H. Lurie Comprehensive Cancer Center of Northwestern University) is appreciated. Instruments in the Northwestern IMSERC facilities were purchased with grants from NSF-NSEC, NSF-MRSEC, Keck Foundation, the state of Illinois, and Northwestern University. We acknowledge the use of instruments in the NU-HTA facilities. We thank Dr. Andrew Mazar for helpful discussions and Mr. Richard Ahn for help with MTS assay.

References

1. Szakacs G, Paterson JK, Ludwig JA, Booth-Genthe C, Gottesman MM. Nat Rev Drug Discov. 2006; 5:219–234. [PubMed: 16518375]
2. Jia J, Zhu F, Ma X, Cao ZW, Li YX, Chen YZ. Nat Rev Drug Discov. 2009; 8:111–128. [PubMed: 19180105]
3. Minotti G, Menna P, Salvatorelli E, Cairo G, Gianni L. Pharmacol Rev. 2004; 56:185–229. [PubMed: 15169927]
4. Wang D, Lippard SJ. Nat Rev Drug Discov. 2005; 4:307–320. [PubMed: 15789122]
5. Kelland L. Nat Rev Cancer. 2007; 7:573–584. [PubMed: 17625587]
6. Martoni A, Bellucco A, Canova N, Pannuti F. Oncology. 1989; 46:109–116. [PubMed: 2710475]
7. Nielsen D, Dombernowsky P, Larsen SK, Hansen OP, Skovsgaard T. Cancer Chemother Pharmacol. 2000; 46:459–466. [PubMed: 11138459]
8. Thigpen JT, Brady MF, Homesley HD, Malfetano J, DuBeshter B, Burger RA, Liao S. J Clin Oncol. 2004; 22:3902–3908. [PubMed: 15459211]
9. Nitiss JL. Nat Rev Cancer. 2009; 9:338–350. [PubMed: 19377506]
10. Bigioni M, Benzo A, Irrissuto C, Lopez G, Curatella B, Maggi C, Manzini S, Crea A, Caroli S, Cubadda F, Binaschi M. Cancer Chemother Pharmacol. 2008; 62:621–629. [PubMed: 18038274]
11. Chou TC, Talalay P. Trends Pharmacol Sci. 1983; 4:450–454.
12. Berenbaum MC. Pharmacol Rev. 1989; 41:93–141. [PubMed: 2692037]
13. Zhao L, Wientjes MG, Au JLS. Clin Cancer Res. 2004; 10:7994–8004. [PubMed: 15585635]
14. Eder JP Jr, Chan VTW, Ng SW, Rizvi NA, Zacharoulis S, Teicher BA, Schnipper LE. Cancer Res. 1995; 55:6109–6116. [PubMed: 8521401]
15. Ali-Osman F, Berger MS, Rajagopal S, Spence A, Livingston RB. Cancer Res. 1993; 53:5663–5668. [PubMed: 8242621]
16. Saleem A, Ibrahim N, Patel M, Li XG, Gupta E, Mendoza J, Pantazis P, Rubin EH. Cancer Res. 1997; 57:5100–5106. [PubMed: 9371509]
17. Peer D, Karp JM, Hong S, Farokhzad OC, Margalit R, Langer R. Nat Nanotechnol. 2007; 2:751–760. [PubMed: 18654426]
18. Davis ME, Chen Z, Shin DM. Nat Rev Drug Discov. 2008; 7:771–782. [PubMed: 18758474]
19. Waterhouse DN, Tardi PG, Mayer LD, Bally MB. Drug Safety. 2001; 24:903–920. [PubMed: 11735647]
20. Lyass O, Hubert A, Gabizon AA. Clin Cancer Res. 2001; 7:3040–3046. [PubMed: 11595693]
21. Ferrero JM, Weber B, Geay JF, Lepille D, Orfeuvre H, Combe M, Mayer F, Leduc B, Bourgeois H, Paraiso D, Pujade-Lauraine E. Ann Oncol. 2007; 18:263–268. [PubMed: 17108151]
22. Rapoport BL, Vorobiof DA, Slabber C, Alberts AS, Hlophe HS, Mohammed C. Int J Gynecol Cancer. 2009; 19:1137–1141. [PubMed: 19820382]
23. Lee SM, Chen H, O'Halloran TV, Nguyen ST. J Am Chem Soc. 2009; 131:9311–9320. [PubMed: 19527027]
24. Lee SM, Chen H, Dettmer CM, O'Halloran TV, Nguyen ST. J Am Chem Soc. 2007; 129:15096–15097. [PubMed: 17999499]
25. Tannock IF, Rotin D. Cancer Res. 1989; 49:4373–4384. [PubMed: 2545340]
26. Li SD, Huang L. Mol Pharm. 2008; 5:496–504. [PubMed: 18611037]
27. Bandak S, Goren D, Horowitz A, Tzemach D, Gabizon A. Anti-Cancer Drugs. 1999; 10:911–920. [PubMed: 10630359]
28. Zamboni W, Gervais A, Egorin M, Schellens JM, Zuhowski E, Pluim D, Joseph E, Hamburger D, Working P, Colbern G, Tonda M, Potter D, Eiseman J. Cancer Chemother Pharmacol. 2004; 53:329–336. [PubMed: 14673619]
29. Harrington KJ, Lewanski CR, Northcote AD, Whittaker J, Wellbank H, Vile RG, Peters AM, Stewart JSW. Ann Oncol. 2001; 12:493–496. [PubMed: 11398881]
30. Kim ES, Lu C, Khuri FR, Tonda M, Glisson BS, Liu D, Jung M, Hong WK, Herbst RS. Lung Cancer. 2001; 34:427–432. [PubMed: 11714540]

31. Casey JR, Grinstein S, Orlowski J. Nat Rev Mol Cell Biol. 2010; 11:50–61. [PubMed: 19997129]
32. Appleton TG, Hall JR, Prenzler PD. Inorg Chem. 1989; 28:815–819.
33. Rice JR, Gerberich JL, Nowotnik DP, Howell SB. Clin Cancer Res. 2006; 12:2248–2254. [PubMed: 16609041]
34. Yde CW, Issinger OG. Int J Oncol. 2006; 29:1397–1404. [PubMed: 17088977]
35. Miller CR, Bondurant B, McLean SD, McGovern KA, O'Brien DF. Biochemistry. 1998; 37:12875–12883. [PubMed: 9737866]
36. Savic R, Luo L, Eisenberg A, Maysinger D. Science. 2003; 300:615–618. [PubMed: 12714738]
37. VanEngeland M, Nieland LJW, Ramaekers FCS, Schutte B, Reutelingsperger CPM. Cytometry. 1998; 31:1–9. [PubMed: 9450519]
38. We note that the mode of cisplatin-induced cell death changed from apoptosis to necrosis above the threshold concentration of cisplatin, due to the significant damage of proteins related to apoptotic process, ultimately leading to necrotic cell death. See reference # 39.
39. Jung Y, Lippard SJ. Chem Rev. 2007; 107:1387–1407. [PubMed: 17455916]
40. Burger KNJ, Staffhorst RWHM, de Vijlder HC, Velinova MJ, Bomans PH, Frederik PM, de Kruijff B. Nat Med. 2002; 8:81–84. [PubMed: 11786911]
41. Maeda H, Wu J, Sawa T, Matsumura Y, Hori K. J Control Release. 2000; 65:271–284. [PubMed: 10699287]
42. Hamelers IHL, van Loenen E, Staffhorst RWHM, de Kruijff B, de Kroon AIPM. Mol Cancer Ther. 2006; 5:2007–2012. [PubMed: 16928821]
43. Dhar S, Gu FX, Langer R, Farokhzad OC, Lippard SJ. Proc Natl Acad Sci USA. 2008; 105:17356–17361. [PubMed: 18978032]
44. Feazell RP, Nakayama-Ratchford N, Dai H, Lippard SJ. J Am Chem Soc. 2007; 129:8438–8439. [PubMed: 17569542]
45. Ahn RW, Chen F, Chen H, Stern ST, Clogston JD, Patri AK, Raja MR, Swindell EP, Parimi V, Cryns VL, O'Halloran TV. Clin Cancer Res. 2010; 16:3607–3617. [PubMed: 20519360]
46. Chen H, Pazicni S, Krett NL, Ahn RW, Penner-Hahn JE, Rosen ST, O'Halloran TV. Angew Chem Int Ed. 2009; 48:9295–9299.
47. Stock RS, Ray WH. J Polym Sci Pt B-Polym Phys. 1985; 23:1393–1447.
48. Appleton TG, Hall JR, Neale DW, Thompson CSM. Inorg Chem. 1990; 29:3985–3990.
49. Haran G, Cohen R, Bar LK, Barenholz Y. Biochim Biophys Acta. 1993; 1151:201–215. [PubMed: 8373796]
50. Lee SM, Ahn RW, Chen F, Fought AJ, O'Halloran TV, Cryns VL, Nguyen ST. ACS Nano. 2010 in press. 10.1021/nn100560p

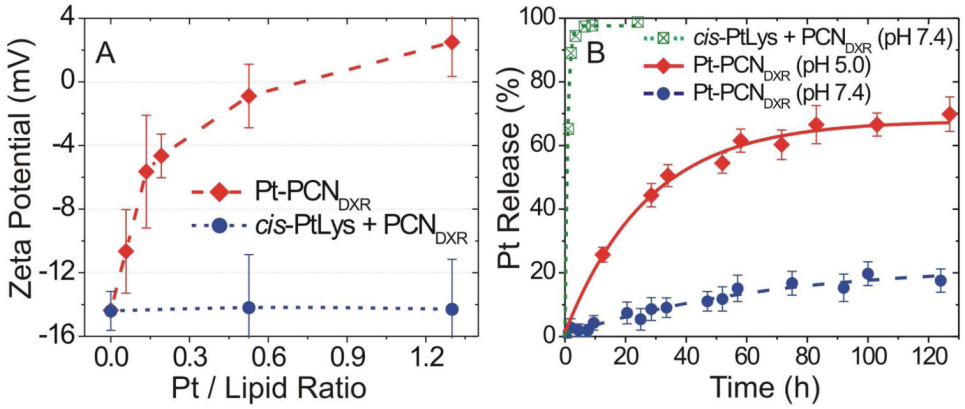

Figure 1.

(A) Zeta (ζ) potential of Pt-PCN$_{DXR}$ with various Pt-to-lipid ratios. (B) pH-responsive Pt-release profiles for Pt-PCN$_{DXR}$ at 37 °C and either pH 5.0 (apparent release rate $k_{5.0}$ = 1.56 h^{-1}) or 7.4 (apparent release rate $k_{7.4}$ = 0.36 h^{-1}). As a control, a dialyzed mixture of *cis*-PtLys and PCN$_{emp}$ rapidly "loses" Pt within a few minutes (green open symbol).

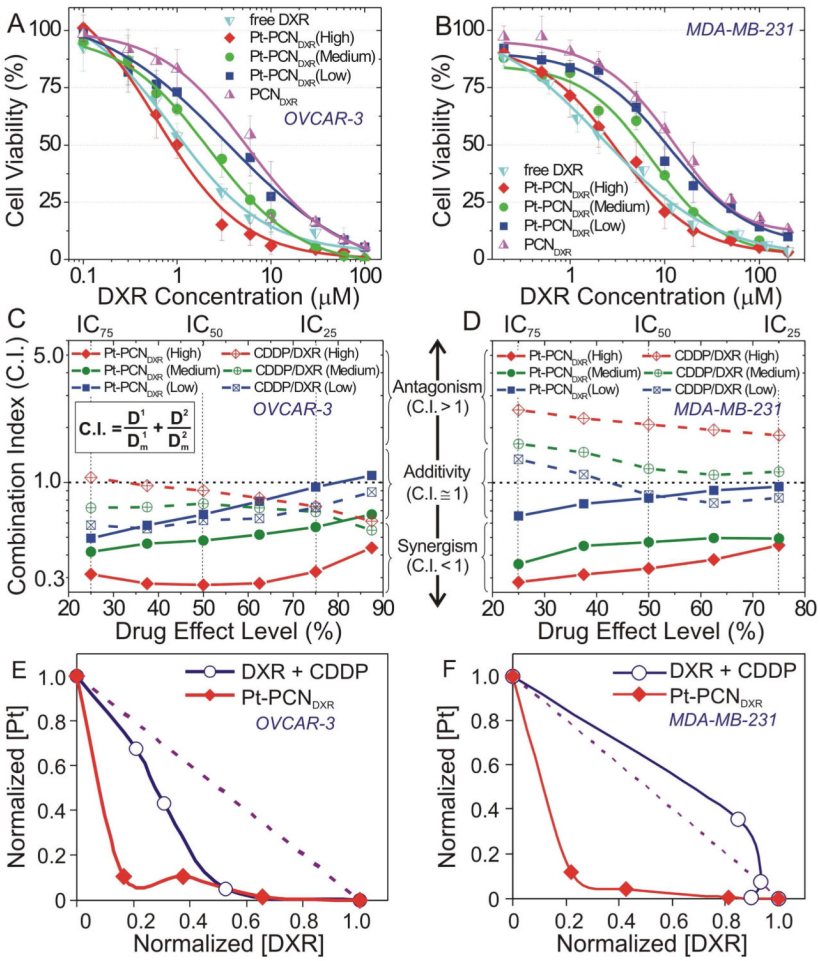

Figure 2.

In vitro cytotoxicity profiles and combination index (C.I.) plots of Pt-PCN$_{DXR}$ with various Pt/DXR ratios as indicated in Table 1. (A, B) Dose-effect profiles for: (A) OVCAR-3 ovarian cancer and (B) MDA-MB-231 breast cancer cells. (C, D) C.I. plots for Pt-PCN$_{DXR}$ (closed symbols) and the free drug combinations (open symbols) against: (C) OVCAR-3 and (D) MDA-MB-231 cells. C.I. values, defined as the sum of the two ratios of the median effect doses (D^1, D^2) of each drug alone to the median effect doses (D^1_m, D^2_m) of each drug in the combination (equation in Inset),[11] were plotted against drug effect levels (IC$_x$ values) at various cell viability points. (E, F) Dose-normalized isobologram analyses based on the iso-effective points at IC$_{50}$ level from dose-effect curves of: (E) OCVAR-3 and (F) MDA-MB-231 cancer cell lines. The dotted diagonal line represents the additivity of orthogonal drug interaction. The data points below or above the line indicate synergistic or antagonistic drug interactions, respectively.

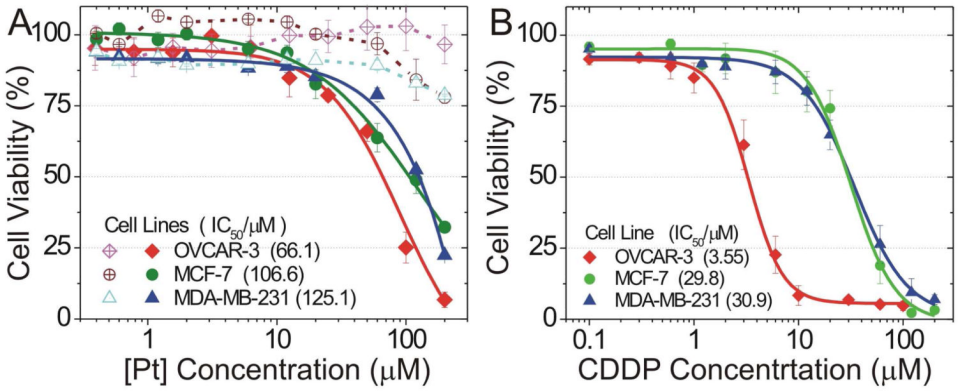

Figure 3. In vitro

cytotoxicity profiles of Pt-PCN_{emp}, *cis*-PtLys, and CDDP. (A) Dose-effect profiles of Pt-PCN_{emp} (closed symbols with solid lines) and free *cis*-PtLys (open symbols with dotted lines) against OVCAR-3, MCF-7, and MDA-MB-231 human cancer cell lines. (B) Dose-effect profiles of cisplatin (CDDP) against OVCAR-3, MCF-7, and MDA-MB-231 cells. Cells were exposed to each drug for 72 h at 37 °C.

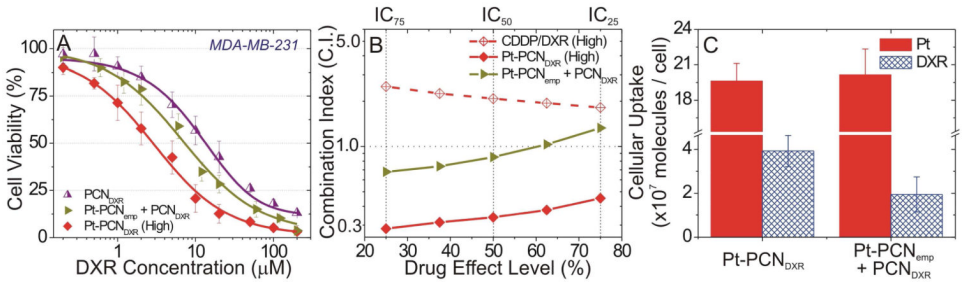

Figure 4.

(A) Dose-effect profiles for MDA-MB-231 breast cancer cells of singly packaged drug combinations [Pt-PCN_{emp} + PCN_{DXR}]. (B) C.I. plots for [Pt-PCN_{emp} + PCN_{DXR}], Pt-PCN_{DXR}, and the free drug combination with the same Pt/DXR ratio against MDA-MB-231 cells. (C) Pt and DXR uptake by MDA-MB-231 cells when exposed to 10 μM solution of Pt-PCN_{DXR} and [Pt-PCN_{emp} + PCN_{DXR}] for 4 h at 37 °C.

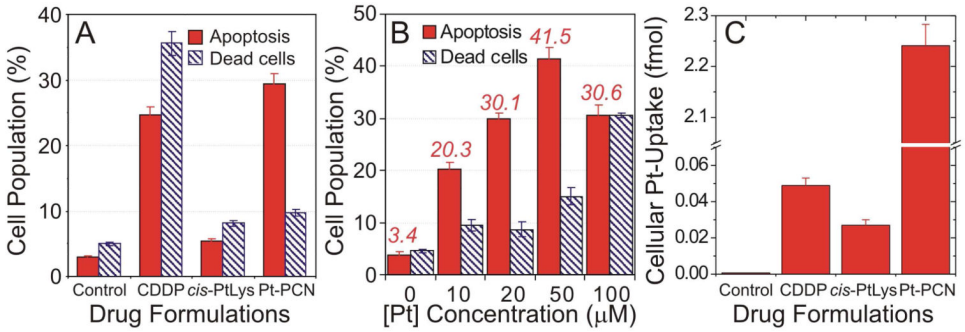

Figure 5.

(A) Apoptotic effect of Pt-drug formulations measured by Annexin-V/7-AAD. OVCAR-3 cells were treated with drug-free media (control), 20 μM solution of free $[Pt^{II}(NH_3)_2(N_{\alpha}$-AcLys)] (*cis*-PtLys), 20 μM solution of cisplatin (CDDP), and 20 μM solution of Pt-conjugated empty PCN (Pt-PCN_{emp}) for 48 h before analyses. (B) Dose-dependent apoptotic effect of Pt-PCN_{emp}. A cumulative bar graph of apoptotic and dead cell populations is presented as a function of the [Pt] concentration in Pt-PCN_{emp}. The average percent populations of apoptotic cells are indicated directly on top of each bar. (C) The Pt uptake by OVCAR-3 cells when exposed to cisplatin (CDDP), $[Pt^{II}(NH_3)_2(N_{\alpha}$-AcLys)] (*cis*-PtLys), and Pt-conjugated PCN_{emp} (Pt-PCN_{emp}). For the control sample (cells grown in media with no exposure to any Pt), Pt was not detected.

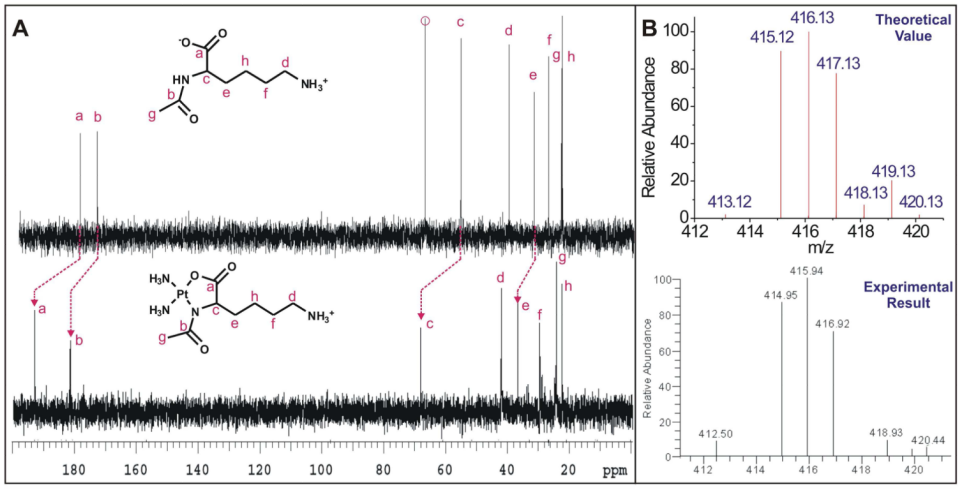

Figure 6.

(A) ^{13}C NMR spectra of N_α-AcetylLysine ligand (top) and $[Pt^{II}(NH_3)_2(N_\alpha\text{-AcLys})]$ (bottom). The carboxylate peak (192.7 ppm, peak 'a' in the bottom spectrum) is characteristic of a deshielded carboxylate peak that is a part of a five-membered chelate ring in Pt compexes.[32,48] The circled peak in the top spectrum is due to dioxane, added to D_2O as a reference. (B) ESIMS isotopic patterns for $[Pt^{II}(NH_3)_2(N_\alpha\text{-AcLys})]$: theoretical (top) and experimental (bottom).

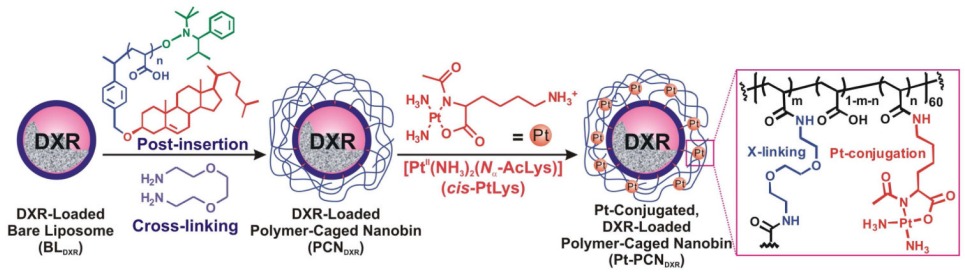

Scheme 1. Preparation of platinum-conjugated, doxorubicin-loaded polymer-caged nanobins (Pt-PCN$_{DXR}$)

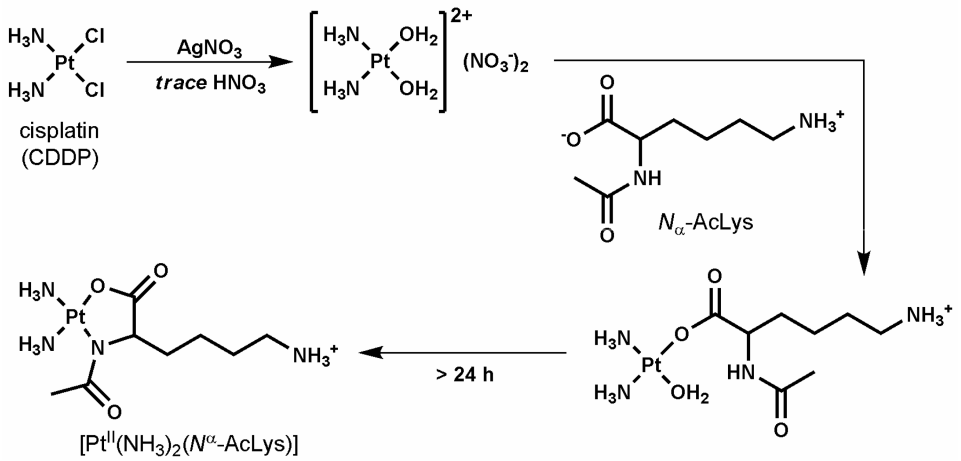

Scheme 2.
Preparation of [$Pt^{II}(NH_3)_2(N_\alpha$-AcLys)](*cis*-PtLys).

Tabel 1

Half-maximal inhibitory concentration (IC_{50}^{DXR} in μM) and the corresponding combination index (C.I.) of Pt-conjugated, DXR-encapsulated polymer-caged nanobins (Pt-PCN_{DXR}) with various Pt/DXR ratios against OVCAR-3 and MDA-MB-231 cancer cell lines.

Drug formulations (Pt-to-DXR ratio)	Pt/DXR ratio	OVCAR-3			Pt/DXR ratio	MDA-MB-231		
		IC_{50}^{DXR}	C.I. (50%)			IC_{50}^{DXR}	C.I. (50%)	
Pt-PCN_{DXR} (High)[a]	5.9 ± 1.1	0.90 ± 0.23	0.27	0.90[b]	5.1± 1.0	2.82 ± 0.98	0.33	2.08[b]
Pt-PCN_{DXR} (Medium)[a]	3.4 ± 0.7	2.03 ± 0.46	0.48	0.77[b]	1.0 ± 0.3	5.58 ± 0.60	0.47	1.19[b]
Pt-PCN_{DXR} (Low)[a]	0.24 ± 0.05	3.55 ± 1.38	0.67	0.62[b]	0.10 ± 0.02	10.6 ± 1.60	0.82	0.86[b]
PCN_{DXR}[a]	-	5.42 ± 1.34	-	-	-	13.1 ± 3.50	-	-
free DXR	-	1.24 ± 0.49	-	-	-	2.54 ± 1.19	-	-
[Pt-PCN_{emp} + PCN_{DXR}[a]]	-	-	-	-	5.1	6.83 ± 1.70	0.85	2.08[b]

[a] DXR/lipid ratio = 0.25 ± 0.03.

[b] C.I. values from free drug combinations at the corresponding Pt/DXR ratio.

J Am Chem Soc. Author manuscript; available in PMC 2013 May 20.

Tabel 2

Half-maximal inhibitory concentration (IC_{50}^{Pt} in μM) of cisplatin (CDDP), Pt-conjugated, empty polymer-caged nanobins (Pt-PCN_{emp}), and *cis*-PtLys from Figure 3.

Drug formulations	Cell lines		
	OVCAR-3	**MDA-MB-231**	**MCF-7**
CDDP	3.55 ± 0.34	30.9 ± 1.23	29.8 ± 1.62
Pt-PCN_{emp} [a]	66.1 ± 2.84	125.1 ± 7.9	106.6 ± 2.69
cis-PtLys	>200	>200	>200

[a] Pt/lipid ratio = 1.29